

Enhanced spontaneous emission inside hyperbolic metamaterials

Lorenzo Ferrari,¹ Dylan Lu,² Dominic Lepage,² and Zhaowei Liu,^{1,2,*}

¹Materials Science and Engineering, University of California, San Diego, 9500 Gilman Drive, La Jolla, California 92093, USA

²Department of Electrical and Computer Engineering, University of California, San Diego, 9500 Gilman Drive, La Jolla, California 92093, USA
[*zhaowei@ucsd.edu](mailto:zhaowei@ucsd.edu)

Abstract: Hyperbolic metamaterials can enhance spontaneous emission, but the radiation-matter coupling is not optimized if the light source is placed outside such media. We demonstrate a 3-fold improvement of the Purcell factor over its outer value and a significant enlargement in bandwidth by including the emitter within a Si/Ag periodic multilayer metamaterial. To extract the plasmonic modes of the structure into the far field we implement two types of 1D grating with triangular and rectangular profile, obtaining a 10-fold radiative enhancement at visible frequencies.

©2014 Optical Society of America

OCIS codes: (160.3918) Metamaterials; (250.5403) Plasmonics; (230.4170) Multilayers; (250.5230) Photoluminescence.

References and links

1. A. Kinkhabwala, Z. F. Yu, S. H. Fan, Y. Avlasevich, K. Mullen, and W. E. Moerner, "Large single-molecule fluorescence enhancements produced by a bowtie nanoantenna," *Nat. Photonics* **3**(11), 654–657 (2009).
2. K. Okamoto, I. Niki, A. Shvartser, Y. Narukawa, T. Mukai, and A. Scherer, "Surface-plasmon-enhanced light emitters based on InGaN quantum wells," *Nat. Mater.* **3**(9), 601–605 (2004).
3. I. De Leon and P. Berini, "Theory of noise in high-gain surface plasmon-polariton amplifiers incorporating dipolar gain media," *Opt. Express* **19**(21), 20506–20517 (2011).
4. A. G. Brolo, "Plasmonics for future biosensors," *Nat. Photonics* **6**(11), 709–713 (2012).
5. H. G. Frey, S. Witt, K. Felderer, and R. Guckenberger, "High-resolution imaging of single fluorescent molecules with the optical near-field of a metal tip," *Phys. Rev. Lett.* **93**(20), 200801 (2004).
6. M. J. Levene, J. Korlach, S. W. Turner, M. Foquet, H. G. Craighead, and W. W. Webb, "Zero-mode waveguides for single-molecule analysis at high concentrations," *Science* **299**(5607), 682–686 (2003).
7. G. Shambat, B. Ellis, A. Majumdar, J. Petykiewicz, M. A. Mayer, T. Sarmiento, J. Harris, E. E. Haller, and J. Vuckovic, "Ultrafast direct modulation of a single-mode photonic crystal nanocavity light-emitting diode," *Nat. Commun.* **2**, 539 (2011).
8. L. Novotny and B. Hecht, *Principles of Nano-optics* (Cambridge University, 2012).
9. G. W. Ford and W. H. Weber, "Electromagnetic-interactions of molecules with metal-surfaces," *Phys. Rep.* **113**(4), 195–287 (1984).
10. W. L. Barnes, "Fluorescence near interfaces: the role of photonic mode density," *J. Mod. Opt.* **45**(4), 661–699 (1998).
11. E. M. Purcell, "Spontaneous emission probabilities at radio frequencies," *Phys. Rev.* **69**, 681 (1946).
12. M. Noginov, M. Lapine, V. Podolskiy, and Y. Kivshar, "Focus issue: hyperbolic metamaterials," *Opt. Express* **21**(12), 14895–14897 (2013).
13. Z. Jacob, I. I. Smolyaninov, and E. E. Narimanov, "Broadband Purcell effect: Radiative decay engineering with metamaterials," *Appl. Phys. Lett.* **100**(18), 181105 (2012).
14. D. Lu, J. J. Kan, E. E. Fullerton, and Z. Liu, "Enhancing spontaneous emission rates of molecules using nanopatterned multilayer hyperbolic metamaterials," *Nat. Nanotechnol.* **9**(1), 48–53 (2014).
15. P. Yeh, *Optical Waves in Layered Media* (Wiley, 1988).
16. P. B. Johnson and R. W. Christy, "Optical constants of the noble metals," *Phys. Rev. B* **6**(12), 4370–4379 (1972).
17. D. E. Aspnes and A. A. Studna, "Dielectric functions and optical parameters of Si, Ge, GaP, GaAs, GaSb, InP, InAs, and InSb from 1.5 to 6.0 eV," *Phys. Rev. B* **27**(2), 985–1009 (1983).
18. S. A. Maier, *Plasmonics: Fundamentals and Applications* (Springer, 2007).
19. P. Berini, "Long-range surface plasmon polaritons," *Adv. Opt. Photonics* **1**(3), 484–588 (2009).

1. Introduction

The enhancement of the recombination rates of point-source emitters represents a strategic objective for nanoplasmonics, given its high impact not only on light generation (single photon sources [1], light emitting diodes [2], and optical amplifiers [3]), but also on a host of other applications ranging from biosensing [4], fluorescence imaging [5] and DNA targeting [6] to the high speed modulation and detection of optical signals [7]. The rate of spontaneous emission (SE) is proportional to the photonic density of states (PDOS), which depends critically on the geometry of the near field [8–10]. Such rate in engineered electromagnetic surroundings can greatly exceed that in a homogeneous dielectric environment, or “free space”, and the ratio of the two constitutes a figure of merit known as Purcell factor [11].

SE enhancement has been demonstrated for a novel class of artificial materials with hyperbolic optical dispersion, therefore referred to as hyperbolic metamaterials (HMM) [12–14]. In contrast to resonant structures like cavities or single metallic/dielectric interfaces, these media exhibit a Purcell factor that is broadband and tunable in frequency. However, emitters dispersed on top of them experience a sharply asymmetrical PDOS, which limits their coupling to the plasmonic modes, and hence the maximum Purcell factor attainable.

In this paper we optimize the SE enhancement of a point source by including it inside a multilayer (ML) silver (Ag)/ silicon (Si) HMM [Fig. 1(a)]. We start in Section 2 by addressing the problem of a point dipole, representing the emitter, placed outside the Ag/Si ML; we calculate the Purcell factor with an analytical model, and use the latter to validate 3D full-wave simulations of the same configuration, obtaining coherent results. After fixing the ML filling ratio, namely the volume percentage of metal in a period, in Section 3 we study the evolution of the Purcell factor as the dipole is embedded within the first five Si layers. Once the optimum configuration is determined, in Section 4 two different kinds of 1D grating, triangular and rectangular, are patterned in the ML [Figs. 1(b) and 1(c)] to outcouple the plasmonic SE components into the far field. In Section 5 we summarize the work done and make final remarks.

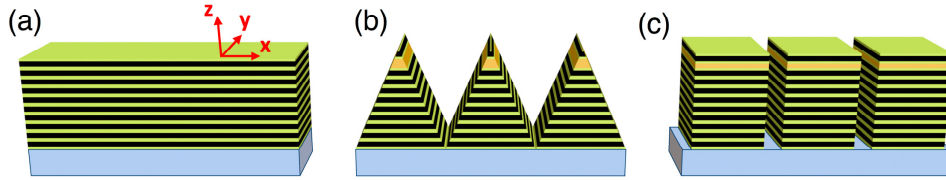


Fig. 1. (a) Uniform Ag/Si ML, (b) triangular and (c) rectangular grating.

2. Emitter outside a uniform Si/Ag ML

We begin our analysis by introducing a model, based on the work of Ford and Weber [9], to compute the SE enhancement of a point source above a uniform (i.e. not patterned) ML. The Purcell factors F_{\parallel} and F_{\perp} of a dipole oriented respectively parallel (\parallel , “p-polarization”) or orthogonal (\perp , “s-polarization”) to the layers and located a distance d above the surface are given by:

$$F_{\parallel} = 1 - \eta_0 \left(1 - \frac{3}{4} \operatorname{Re} \int_0^{\infty} dk_{\parallel} D_{\parallel}(k_{\parallel}) \right). \quad (1)$$

$$F_{\perp} = 1 - \eta_0 \left(1 - \frac{3}{2} \operatorname{Re} \int_0^{\infty} dk_{\parallel} D_{\perp}(k_{\parallel}) \right). \quad (2)$$

where the power density spectra $D_{\parallel}(k_{\parallel})$ and $D_{\perp}(k_{\parallel})$ are defined as:

$$D_{\parallel} = \frac{1}{k_z} \frac{k_{\parallel}}{\sqrt{\varepsilon_1 k_0}} \left[1 + r_s e^{2ik_z d} + \left(\frac{k_z}{\sqrt{\varepsilon_1 k_0}} \right)^2 (1 - r_p e^{2ik_z d}) \right]. \quad (3)$$

$$D_{\perp} = \frac{1}{k_z} \left(\frac{k_{\parallel}}{\sqrt{\varepsilon_1 k_0}} \right)^3 (1 + r_p e^{2ik_z d}). \quad (4)$$

In the formulae above, η_0 denotes the internal quantum efficiency of the dipole in a free space with real permittivity ε_1 (and is assumed to be unity in our calculations), $k_0 = \frac{2\pi}{\lambda_0}$ is the magnitude of the wavevector in vacuum at wavelength λ_0 , $k_{\parallel} = \sqrt{k_x^2 + k_y^2}$ and $k_z = \sqrt{\varepsilon_1 k_0^2 - k_{\parallel}^2}$ are the wavevector components along the in-plane and vertical directions respectively, and r_p , r_s represent the amplitude reflection coefficients of the ML for a P- (TM) or S- (TE) polarized plane wave (not to be confused with the dipole polarization), retrieved with a transfer matrix method (TMM) [15]. Dipoles occurring in nature are isotropic [8]; therefore a more appropriate Purcell factor F_{iso} is obtained through an average over F_{\parallel} and F_{\perp} :

$$F_{iso} = \frac{1}{3} (F_{\perp} + 2F_{\parallel}). \quad (5)$$

where the factor 2 accounts for the two equivalent orthogonal in-plane orientations.

We consider a ML composed of 10 Ag/Si periods, each 20 nm thick; the uppermost Ag layer is capped by a 5 nm Si “matching layer”, and the entire structure is sandwiched between two semi-infinite glass regions. A dipole with p- or s- polarization is placed 10 nm above the Si “matching layer”, the purpose of which is to ensure the correct plasmonic coupling at the first interface (Si-Ag, and not glass-Ag). The permittivity of glass is taken to be $\varepsilon_1 = 2.25$, whereas those of Ag and Si are extracted respectively from [16] and [17]. Figure 2(a) illustrates the tunability properties of the ML, computed with Matlab. When the metal filling ratio ρ of a period is decreased from 100%, the Purcell peak is broadened by the higher number of plasmonic modes made available to the emitter. Such modes originate from the hybridization of the resonances associated to individual Ag/Si interfaces, as the latter are brought together in a ML, very much like the case of electrons or phonons in solids, or dielectric slabs in photonic crystals. In the power density spectra of Figs. 2(b)–2(d) we observe distinctly the transition between two limit behaviors: a single metallic interface (volume fraction $\rho = 1$) supports only one resonance [Fig. 2(b)]; on the other hand, minimizing the percentage of metal in a period [Figs. 2(c) and 2(d)] reduces each Ag layer to a thin film sandwiched between two thick Si slabs. Accordingly, the modes tend to group and merge into the even and odd branches manifested by an insulator-metal-insulator (IMI) geometry [18,19]. We also notice that, irrespective of the filling ratio, all the modes converge to the single interface resonance [$\lambda_0 = 360$ nm for Ag/glass, Fig. 2(b), and $\lambda_0 = 594$ nm for Ag/Si, Figs. 2(c) and 2(d)]; as a consequence of the mode separation discussed above, the convergence is faster for large filling ratios, while it happens at higher wavevectors for the small ones.

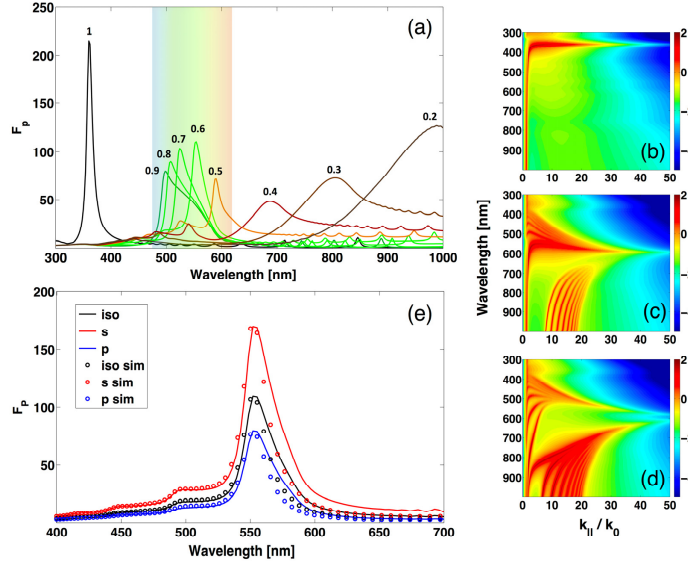


Fig. 2. (a) Purcell factor F_P for an isotropic dipole in glass 10 nm above the Si/Ag uniform ML. The Ag volume fraction ρ is varied from 1 (in which case the Si capping layer is excluded) to 0.2, as indicated above each curve. The tunability is finer in the yellow-green region of the visible range, highlighted by the colored background. (b) Power density spectrum (logarithmic scale) of an s- dipole for $\rho = 1$, (c) 0.6 and (d) 0.3. (e) Comparison between the Purcell factors of an s-, p- and isotropic dipole with $\rho = 0.6$, obtained with analytical calculations (continuous curves) and FDTD simulations (open circles).

In view of the extension of our study to the inside of the ML, we perform 3D full-wave finite-difference time-domain (FDTD) simulations on a cluster with the commercial software Comsol Multiphysics. We reproduce the configuration adopted in the analytical calculations using the same geometric and material parameters, and evaluate the Purcell factor as:

$$F_{\parallel,\perp} = \frac{P_{\parallel,\perp}^{ML}}{P^0} = \frac{P_{\parallel,\perp}^r + P_{\parallel,\perp}^{nr}}{P^0}. \quad (6)$$

where P_{\parallel}^{ML} (P_{\perp}^{ML}) is the total power emitted by a parallel (orthogonal) electric point dipole 10 nm above the ML, sum of the power P_{\parallel}^r (P_{\perp}^r) radiated into the far field and the power P_{\parallel}^{nr} (P_{\perp}^{nr}) dissipated into the structure; P^0 is the total power emitted by the dipole in free space. The isotropic source behavior is again mimicked as in Eq. (5).

We choose to focus on the $\rho = 0.6$ filling ratio, corresponding to 12 nm of Ag and 8 nm of Si, which yields the highest Purcell factor (110-fold enhancement at $\lambda_0 = 554$ nm) in the visible range. Figure 2(e) shows a good agreement between analytical and FDTD results, so that hereafter we will confidently carry out our investigation by means of 3D simulations.

3. Emitter inside a uniform Si/Ag ML

The transition of the source to the center of the Si layers, as depicted in Fig. 3(a), strengthens and enriches the spectral response of the ML, calculated for a parallel, orthogonal and isotropic dipole [Figs. 3(b)–3(d)]. First, the maximum Purcell factor is enhanced up to 3-fold (at $\lambda_0 = 554$ nm) with respect to its value outside the structure, since the emitter now interacts with two high-PDOS regions rather than just one. Including the source in the middle of the Si films makes the host medium coincide with the non-metallic constituent of the ML. This eliminates the need for the “matching layer” discussed in Section 2 and promotes a more efficient coupling, as the distance between the emitter and the first accessible Si/Ag interfaces

is reduced. Second, the Purcell factors related to Position 1 in Figs. 3(b) and 3(c) do not discriminate the orientation of the dipole except for a different peak intensity [10], observed in proportion also in the other positions. The SE enhancement of an internal emitter manifests instead a polarization-dependent spectral signature, which can be explained with a simple symmetry argument.

When a p-dipole is embedded in the middle of a Si layer, its electric field components along the opposing Ag/Si interfaces [green arrows in the inset of Fig. 3(b)] possess inversion and mirror-image symmetry; an s-dipole still exhibits the former, but its mirror image is antisymmetric [inset of Fig. 3(c)]. Therefore, a parallel polarization excites the odd modes lying at shorter wavelengths than the Ag/Si resonance, while a perpendicular polarization activates both the odd and the even ones, the latter resulting more pronounced. The isotropic response of Fig. 3(d) originates from the weighted overlap of these purely symmetric and hybrid contributions.

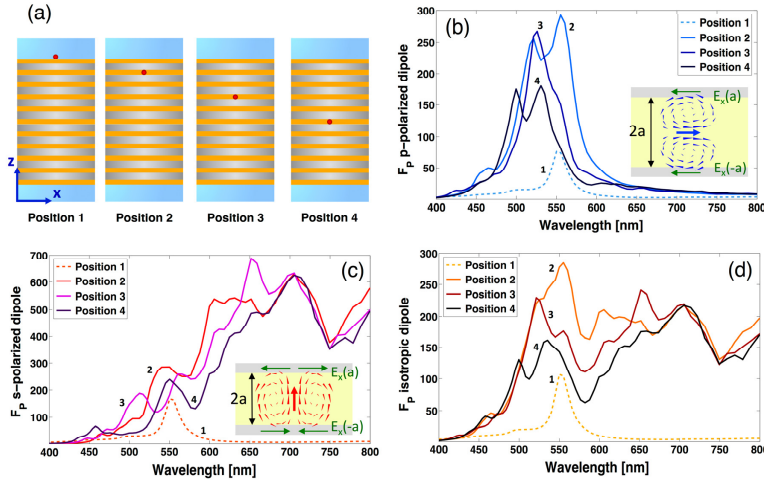


Fig. 3. (a) Positioning of a dipole (indicated by a red dot) outside and inside selected Si layers (ochre stripes) of the uniform ML. (b) Purcell factor F_p of a parallel or (c) orthogonal dipole for the outer (dashed line) and inner positions (solid lines). The insets show the coupling of the dipole field, directed from the tail to the tip of the triangles and proportional in magnitude to their size, to the Ag (grey)/Si (yellow) interfaces. (d) Purcell factor of an isotropic emitter for the positions considered in (b) and (c).

4. Emitter inside a 1D-nanopatterned Si/Ag ML

In order to scatter the plasmonic modes into the far field [18], we design a 1D grating, with either triangular or rectangular profile as sketched in Figs. 1(b) and 1(c). We quantify the far field radiative enhancement as:

$$RE(\theta) = \frac{P_{\uparrow}^r(\theta)}{P_{\uparrow}^0(\theta)}. \quad (7)$$

where $P_{\uparrow}^r(\theta)$ and $P_{\uparrow}^0(\theta)$ are the powers emitted by a dipole respectively inside the ML and in free space into a cone with vertex in the emitter, axis oriented as the positive z direction and half-angle θ . The presence of the grating breaks the in-plane symmetry of the uniform ML, so that both the Purcell factor and the radiative enhancement of an isotropic source are retrieved through an average over the three Cartesian polarizations:

$$F_{iso} = \frac{1}{3}(F_x + F_y + F_z), \quad RE_{iso} = \frac{1}{3}(RE_x + RE_y + RE_z). \quad (8)$$

We fix the dipole in Position 2, and set the emitting layer and the outer region material to polymethyl methacrylate (PMMA). The first replacement introduces an alternative host to Si that is easier to dope with emitters active at the considered frequencies; the second makes optically homogeneous all the volume unoccupied by the ML, so that any changes in the directionality and intensity of radiation with respect to free space can be attributed exclusively to the outcoupling structures. Accordingly, we add above and below the emitting region two 5 nm Si “matching layers”, in contact respectively with 1 and 9 periods with $\rho = 0.6$.

We implement a triangular grating with a pitch of 300 nm, and a rectangular grating with a pitch of 200 nm and a slit width of 40 nm. After optimizing the computational and geometric parameters, the emitting region thickness is set to 20 nm for the first structure, and to 10 nm for the second. A dipole centered in the emitting layer of an individual grating period experiences the Purcell factors displayed in Fig. 4(a). The response of the triangular grating with a 20 nm PMMA layer (blue curve) is similar to that of a uniform ML with an emitting region of identical thickness (red curve), which demonstrates the weak effect of nanopatterning on the SE enhancement. The radiative enhancements induced by the gratings [Figs. 4(b) and 4(c)] are both red-shifted, and extend over a slightly wider region than the Purcell peak of Fig. 4(a); we observe the highest displacement and spread in the rectangular structure. They also increase as the collection angle θ is decreased, with a gradient dictated by the grating geometry. The triangular nanopattern allows a maximum radiative enhancement of about 10 at $\lambda_0 = 576$ nm and $\theta = 35^\circ$, while the rectangular one reaches almost a 6-fold enhancement at $\lambda_0 = 582$ nm and $\theta = 35^\circ$.

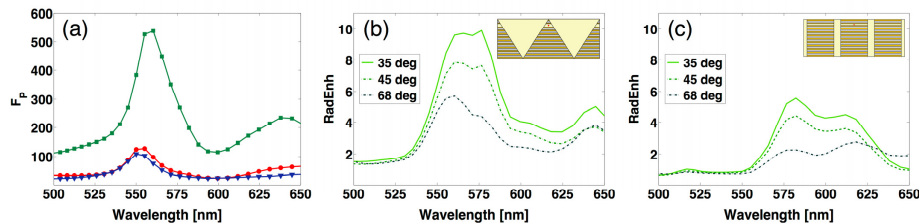


Fig. 4. (a) Isotropic Purcell factor for the triangular grating (blue curve, triangular markers), the rectangular grating (green curve, square markers) and an unpatterned structure with an emitting layer of 20 nm (red curve, circular markers). (b) Radiative enhancement at different angles for an isotropic dipole, provided by the triangular grating, and (c) by the rectangular grating, sketched in the insets.

5. Conclusions

We investigated the SE enhancement of a point source as a function of its position inside a HMM, consisting of a 10 period Ag/Si ML. We first tuned via filling ratio the Purcell factor over the visible spectrum, and explained how plasmonic modes arise from the hybridization of the individual Ag/Si interfaces. Next, we introduced the emitter in the inner semiconducting layers, and observed that the Purcell spectral response derives from the orientation-selective coupling of the dipole with the modes. The isotropic SE enhancement inside the ML reaches a maximum of almost 300-fold, 3 times larger than its peak value for an external emitter. Finally, we proposed two 1D gratings to extract into the far field the plasmonic components of the emission spectrum, obtaining a radiative enhancement as high as 10-fold. Future work will include a study of alternative outcoupling mechanisms, together with the fabrication and characterization of the examined structures.

Acknowledgment

The authors would like to acknowledge financial support from ONR Young Investigator Award (#N00014-13-1-0535).